FLOMEKO 2003
11th IMEKO TC9 Conference on Flow Measurement
Groningen, NETHERLANDS, 12 - 14 May 2003

THE CHARACTERISTICS OF THE STRAIGHT-TUBE CORIOLIS FLOWMETER FOR DIFFERENT LATERAL VIBRATION MODES

Jože Kutin, Ivan Bajsic
Laboratory of Measurements in Process Engineering, Faculty of Mechanical Engineering, University of Ljubljana, Slovenia

The aim of this theoretical paper is to discuss and compare the measuring characteristics of the Coriolis meter with a straight and slender measuring tube for the lowest three lateral vibration modes. The work is based on an analysis of the analytical approximations of the meter's characteristics, which are derived from the solutions of a one-dimensional mathematical model. The paper deals separately with the ideal characteristics, the stability-boundary effect, the axial-force effect and the added-masses effect. The influence of the motion sensors' position is stressed in the presentation of the results.

1. INTRODUCTION

The Coriolis meter is used for measuring the mass flowrate and the density of fluids. Its operation is based on the alteration of the mode shape and the natural frequency of the vibrating measuring tube. This paper is focused on the configuration with a straight and slender measuring tube. In most cases such Coriolis meters make use of the fundamental, i.e. the first lateral vibration mode. However, the higher vibration modes are also under the influence of the same measuring effects, so they can, in general, also be employed. An interesting possibility is represented by a simultaneous application of two or more vibration modes. The measuring results from the additional modes can be used for correcting or identifying undesired effects on the meter's operation. As an example, see the patent document [1], which suggests the possibility of eliminating the fluid-pressure effect by taking account of its different influence on two modes.

The application of the higher modes requires a knowledge of the associated measuring characteristics. In this theoretical paper, the basic measuring effects of the straight-tube Coriolis meter, including the effects of the stability boundary, the axial force and the added masses, are compared for the lowest three vibration modes. The contents follow the authors' previous work (see, e.g. Refs. [2, 3]), where the meter's approximate characteristics were derived in an analytical form. The obtained relations are valid for any of the vibration modes, but discussion of the results was previously limited to the first one. The characteristics of the higher modes were already included in the studies of other authors (see, e.g. Refs. [4-7]); however, in presenting this paper we can offer some additional findings and new conclusions. The presentation of the results in the next sections is aimed at showing the influence of the motion sensors' position, the choice which is very important for the particular mode.

2. THE MATHEMATICAL MODEL

The model of the Coriolis meter under discussion is schematically presented in Fig. 1. The fluid being measured flows through a straight and slender measuring tube, which is clamped at both ends. Taking into account that only the resonance conditions of the measuring tube are of interest and the vibration damping is relatively small, the mathematical model is reduced to a description of the undamped free motions. Applying the theories of the Euler beam and one-dimensional fluid flow, its equation of motion and boundary conditions can be written as:

$$\frac{\partial^4\eta}{\partial\xi^4}+\left(\beta\upsilon^2+\Pi\right)\frac{\partial^2\eta}{\partial\xi^2}+2\beta\upsilon\frac{\partial^2\eta}{\partial\xi\partial\tau}+\left(1+\beta+\sum_j\alpha_j\,\delta\left(\xi-\xi_j\right)\right)\frac{\partial^2\eta}{\partial\tau^2}=0\,, \tag{1}$$

$$\eta=\frac{\partial\eta}{\partial\xi}=0 \quad \text{at} \quad \xi=0\,,\ \xi=1\,, \tag{2}$$

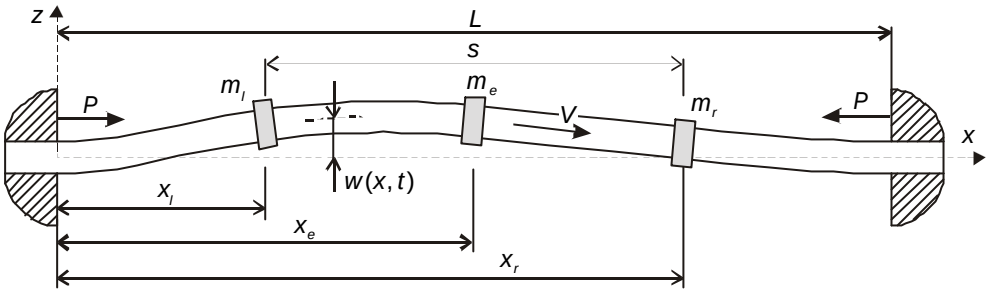

Fig. 1. Model of the straight, slender tube Coriolis meter.

where a dimensionless notation with the reduction on the tube's parameters (the length L, the mass per unit length M_t and the flexural rigidity EI) has been used:

$$\eta = \frac{w}{L},\ \xi = \frac{x}{L},\ \tau = \frac{t}{L^2}\sqrt{\frac{EI}{M_t}},\ \beta = \frac{M_f}{M_t},\ \upsilon = VL\sqrt{\frac{M_t}{EI}},\ \Pi = \frac{PL^2}{EI},\ \alpha_j = \frac{m_j}{LM_t}. \tag{3}$$

The dimensionless quantities in the above equation, from left to right, are related to the tube's lateral deflection $w(x,t)$, the axial coordinate x, the time t, the fluid mass per unit length M_f, the fluid mean axial velocity V, the compressive axial force P and the additional point masses m_j of the exciter, left sensor and right sensor ($j = e$, l and r, respectively).

Using the Rayleigh-Ritz method, the solution for the tube's vibration, which is harmonic in time, may be expressed in a complex form as:

$$\eta(\xi,\tau) = \sum_n A_n \varphi_n(\xi)\exp(i\Omega\tau), \tag{4}$$

where Ω is the dimensionless vibration frequency and φ_n are the comparison functions, which have to satisfy all the boundary conditions. In our case, the Euler-beam modal functions with clamped-clamped boundary conditions (2) were chosen, which represents the exact solutions of Eq. (1), excluding the effects of fluid flow, axial force and added masses:

$$\varphi_n(\xi) = \cosh\lambda_n\xi - \cos\lambda_n\xi - \frac{\cosh\lambda_n - \cos\lambda_n}{\sinh\lambda_n - \sin\lambda_n}(\sinh\lambda_n\xi - \sin\lambda_n\xi). \tag{5}$$

The λ_n values result from equation $\cos\lambda\cosh\lambda = 1$. If Eq. (4) is substituted into Eq. (1), and the result is multiplied by φ_m, and then integrated with respect to ξ from 0 to 1, one obtains a homogeneous system of linear equations:

$$\mathbf{YA} = \mathbf{0},\ Y_{mn} = \left(\lambda_m{}^4 - (1+\beta)\Omega^2\right)c_{mn} + 2\beta\upsilon\Omega i d_{mn} - \left(\beta\upsilon^2 + \Pi\right)e_{mn} - \Omega^2\sum\nolimits_j \alpha_j f_{mn}(\xi_j), \tag{6}$$

with the constants c_{mn}, d_{mn}, e_{mn} and $f_{mn}(\xi_j)$ given in the Appendix, Eqs. (A.1) and (A.2). The condition for nontrivial solutions, $\det\mathbf{Y} = 0$, represents an equation for the natural frequencies Ω_k. By choosing the mode of interest, the constants A_m can be calculated. The actual deflection is determined as the real part of the supposed complex solution:

$$\eta_k(\xi,\tau) = \Phi_k(\xi)\cos\left(\Omega_k\tau + \phi_k(\xi)\right), \tag{7}$$

where Φ_k is the normalized vibration amplitude and ϕ_k is the initial phase.

3. MEASURING CHARACTERISTICS

The measured quantities in the Coriolis meter, i.e. the mass flowrate and the density of the fluid, can be described by the parameters $\beta\upsilon$ and β in the dimensionless form. The fluid density is measured using its influence on the tube's natural frequency Ω_k, and the mass flowrate is determined by measuring the phase difference $\Delta\phi_k$ or time difference $\Delta\tau_k$ between the signals from the symmetrically located motion sensors at ξ_l and ξ_r (the distance between them is $\sigma = s/L$):

$$\Delta\phi_k = \phi_k(\xi_r) - \phi_k(\xi_l), \quad \Delta\tau_k = \frac{\Delta\phi_k}{\Omega_k}. \tag{8}$$

Analytical approximations of the meter's characteristics will be derived by applying a Taylor series expansion to the solutions of the Rayleigh-Ritz method. All the numerical results will be calculated by summing up a sufficient number of terms in the Rayleigh-Ritz series to ensure convergence. The analysis is limited to the lowest three modes (k = 1, 2 and 3), for which the meter's sensitivity under ideal conditions will be studied, proceeded with the effects of the stability boundary, the axial force and the added masses.

3.1 Ideal characteristics

Under some ideal circumstances, the Coriolis meter enables independent measurements of the fluid density and the mass flowrate. Such ideal characteristics can be derived by neglecting the axial-force and added-masses terms in the mathematical model, and then linearizing the solutions for the natural frequency and time difference with respect to the fluid velocity:

$$\Omega_k^{(id)} = \frac{g_{\Omega,k}}{\sqrt{1+\beta}}, \quad \Delta\tau_k^{(id)} = h_{\Delta\tau,k}\beta\upsilon, \tag{9}$$

where $g_{\Omega,k}$ and $h_{\Delta\tau,k}$ are calibration constants of a particular vibration mode k (see Appendix, Eq. (A.3)). Although the natural frequencies increase for higher modes,

$$g_{\Omega,1} / g_{\Omega,2} / g_{\Omega,3} = 1/2.76/5.40, \tag{10}$$

their relative sensitivity to the fluid density β remains unchanged:

$$\frac{1}{\Omega_k}\frac{d\Omega_k}{d\beta} = \frac{-1}{2(1+\beta)}. \tag{11}$$

As shown in Fig. 2, the meter's sensitivity on the mass flowrate $h_{\Delta\tau,k}$ is significantly affected by the motion sensor's position. If the Euler-beam modal functions φ_k are also presented (Fig. 3), it is evident that the time differences increase when approaching the vibration nodes and the tube supports. Because measuring the time or phase difference from relatively small signals is more problematic (because of a smaller signal-to-noise ratio), the diagrams in Fig. 2 cannot represent the basis for choosing the appropriate distance between the sensors. Following Ref. [8], the optimum distance $\sigma_{opt,k}$ can be defined as the maximum of the product of the meter's sensitivity

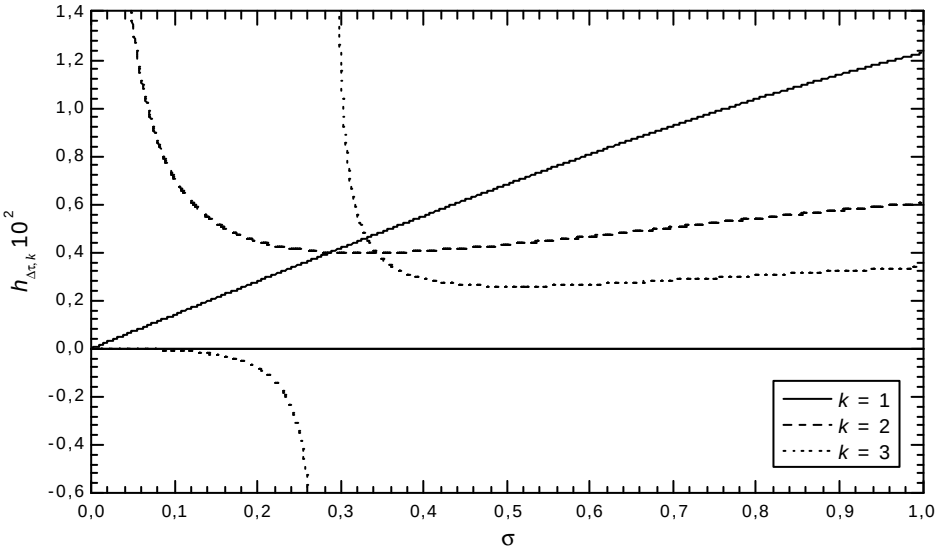

Fig. 2: Variation of the meter's sensitivity $h_{\Delta\tau,k}$ with the sensors' distance for the lowest three modes.

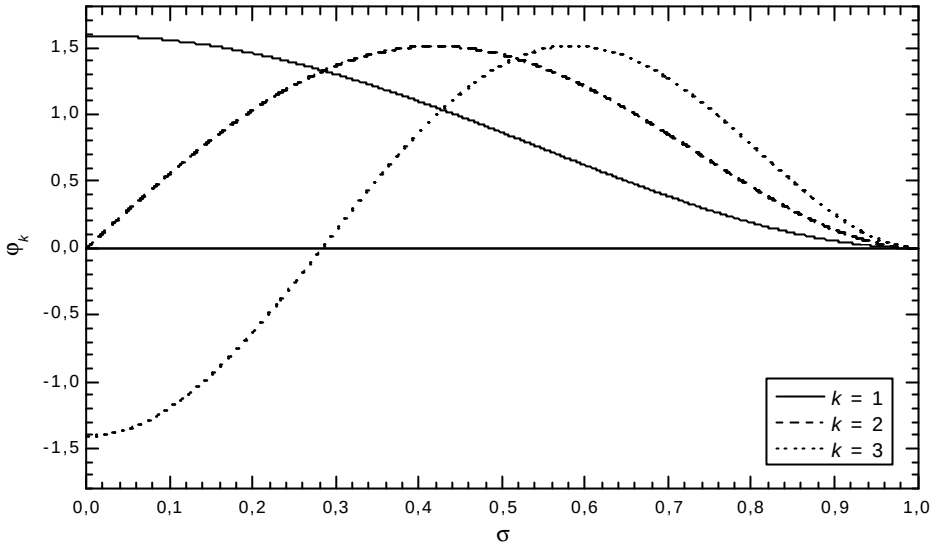

Fig. 3: Variation of the modal functions φ_k with the sensors' distance for the lowest three modes.

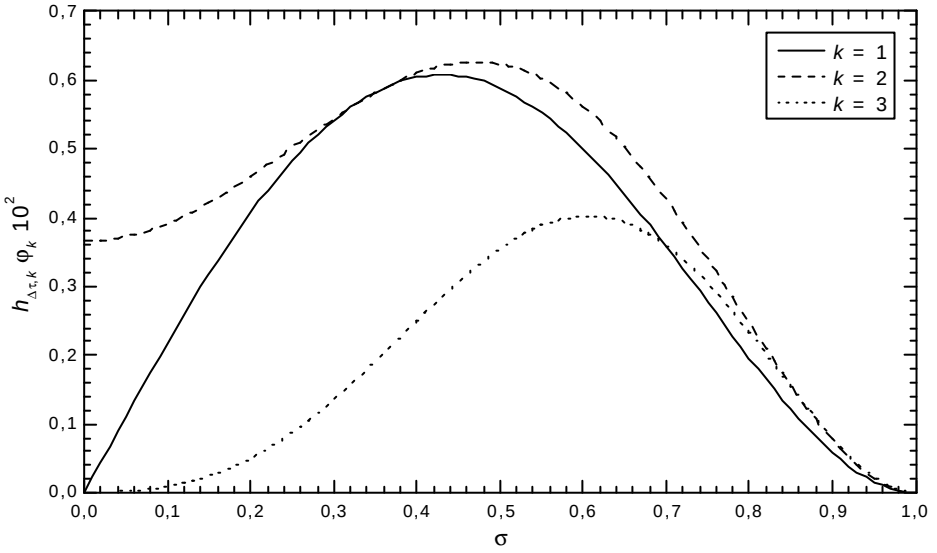

Fig. 4: Variation of the product $h_{\Delta\tau,k}\varphi_k$ with the sensors' distance for the lowest three modes.

and the vibration amplitude, e.g. $h_{\Delta\tau,k}\varphi_k$. Fig. 4 shows that this product reaches its maximum value at:

$$\sigma_{opt,1} = 0.430,\ \sigma_{opt,2} = 0.470,\ \sigma_{opt,3} = 0.606, \tag{12}$$

for the lowest three modes, respectively. Considering such positions of the motion sensors, the ratios between the meter sensitivities for the particular modes are:

$$h_{\Delta\tau,1} / h_{\Delta\tau,2} / h_{\Delta\tau,3} = 1/0.72/0.45\ . \tag{13}$$

The time difference is often determined indirectly, by measuring the phase difference between the sensors' signals. In this case the sensitivity that is important for the mass-flowrate measurement is:

$$h_{\Delta\phi,k} = h_{\Delta\tau,k}\Omega_k^{(id)}\ , \tag{14}$$

and the ratios become:

$$h_{\Delta\phi,1} / h_{\Delta\phi,2} / h_{\Delta\phi,3} = 1/2.0/2.5 . \tag{15}$$

From this we can conclude that, in view of the phase difference, the higher modes can offer the meter a higher sensitivity to the mass flowrate.

3.2 The stability-boundary effect

The stability-boundary effect leads to the dependence of the mass-flowrate and fluid-density measurements, in cases when the fluid velocity is not small enough with respect to the critical velocity $\upsilon_{cr,k}$, at which the vibrating system becomes unstable. Neglecting the axial-force and added-masses terms in the mathematical model, this effect can be estimated by expanding the Taylor series for the natural frequency and the time difference up to the quadratic terms:

$$\Omega_k = \Omega_k^{(id)} \sqrt{1 - \left(g_{cen,k} + g_{cor,k} \frac{\beta}{1+\beta} \right) \beta \upsilon^2} \ , \ \Delta\tau_k = \Delta\tau_k^{(id)} \left[1 + \left(h_{cen,k} + h_{cor,k} \frac{\beta}{1+\beta} \right) \beta \upsilon^2 \right], \tag{16}$$

where $g_{cen,k}$ and $g_{cor,k}$ are constant for a particular k, but $h_{cen,k}$ and $h_{cor,k}$ additionally depend on the position of the motion sensors (see Appendix, Eq. (A.4)). The non-idealities can be interpreted as the effect of the centrifugal force (terms with $g_{cen,k}$ and $h_{cen,k}$) and the higher-order effect of the Coriolis force (terms with $g_{cor,k}$ and $h_{cor,k}$). Further introducing:

$$g_{cr,k} = g_{cen,k} + g_{cor,k} \frac{\beta}{1+\beta} , \ h_{cr,k} = h_{cen,k} + h_{cor,k} \frac{\beta}{1+\beta} , \tag{17}$$

the values of $g_{cr,k}$ are calculated for the lowest three modes:

$$\beta = 0 : \ g_{cr,1} = 2.46 \cdot 10^{-2} , \ g_{cr,1} / g_{cr,2} / g_{cr,3} = 1/0.49/0.28 ,$$
$$\beta = \infty : \ g_{cr,1} = 3.82 \cdot 10^{-2} , \ g_{cr,1} / g_{cr,2} / g_{cr,3} = 1/0.26/0.13 , \tag{18}$$

and the values of $h_{cr,k}$ are presented in Fig. 5 with regard to the sensor's distance. In general, the higher modes are characterized by the smaller stability-boundary non-idealities, which can be explained by the higher critical velocities. For example, the ratio between the critical velocities for the lowest three modes and β = 0.1 is:

$$\frac{1}{\upsilon_{cr,1}^{\ 2}} / \frac{1}{\upsilon_{cr,2}^{\ 2}} / \frac{1}{\upsilon_{cr,3}^{\ 2}} = 1/0.49/0.25 . \tag{19}$$

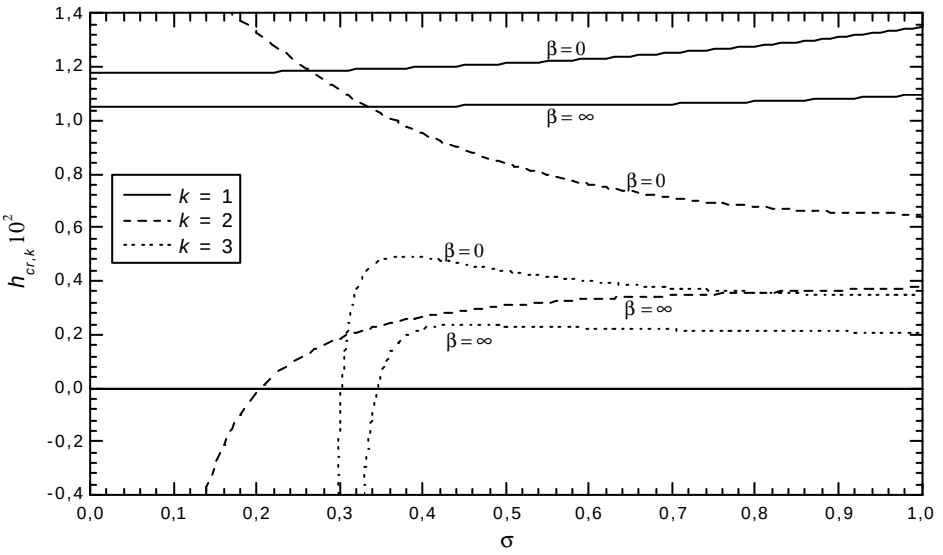

Fig. 5: Variation of the constant $h_{cr,k}$ referring to the stability-boundary effect with the sensors' distance for the lowest three modes.

3.3 The axial-force effect

The axial force acting on the measuring tube may be the consequence of the tube's pre-stress, temperature tension, internal pressurization by the fluid, etc. The influence of this force can be estimated from the linearization of the meter's characteristics with respect to Π:

$$\Omega_k = \Omega_k^{(id)}\sqrt{1 - g_{cen\,k}\Pi}\,, \quad \Delta\tau_k = \Delta\tau_k^{(id)}\left(1 + h_{cen\,k}\Pi\right), \tag{20}$$

where the added masses were also neglected and the fluid velocity was assumed to be relatively small. The axial-force effect has an identical form to the centrifugal-force term in Eq. (16). Therefore, its magnitude can be determined from Eq. (18), for the fluid-density characteristic, and from Fig. 5, for the mass-flowrate characteristic, considering $\beta = 0$ ($g_{cr,k} = g_{cen,k}$, $h_{cr,k} = h_{cen,k}$). It can be concluded that the use of the higher modes would result in the Coriolis meter being less sensitive to variations in the axial force.

3.4 The added-masses effect

The magnitude of the point masses is defined by the weights of the motion sensors and the vibration exciters, which are directly attached to the tube. The parameter α_j represents the ratio of the point mass to the measuring tube's mass. The influence of such added masses can be approximated by linearizing the meter's characteristics with respect to α_j. For the natural frequency it is physically correct to linearize the term under the square root of the denominator that represents the mass of the vibrating system. In addition, neglecting the axial-force and the stability-boundary effects, one obtains:

$$\Omega_k = \Omega_k^{(id)}\sqrt{\frac{1}{1 + \dfrac{1}{1+\beta}\sum_j f_{kk}(\xi_j)\,\alpha_j}}\,, \quad \Delta\tau_k = \Delta\tau_k^{(id)}\left(1 + \frac{1}{1+\beta}\sum_j h_{j,k}\alpha_j\right), \tag{21}$$

where $h_{j,k}$ is a constant for a particular mode k and the positions of the masses (see Appendix, Eq. (A.5)). The natural frequency is decreased under the influence of the added masses. Its variation is larger if the point masses are located in the range of large vibration amplitudes, $f_{kk} = \varphi_k^2$. Considering the added masses, the time difference and, as a consequence, the mass-flowrate characteristic become generally dependant on the fluid density. Figs. 6, 7 and 8 show the relation between the values of $\sum_j h_{j,k}$ and the measuring distance σ for three different combinations of the added masses. It is evident that the higher modes can tend to result in (up to an order of

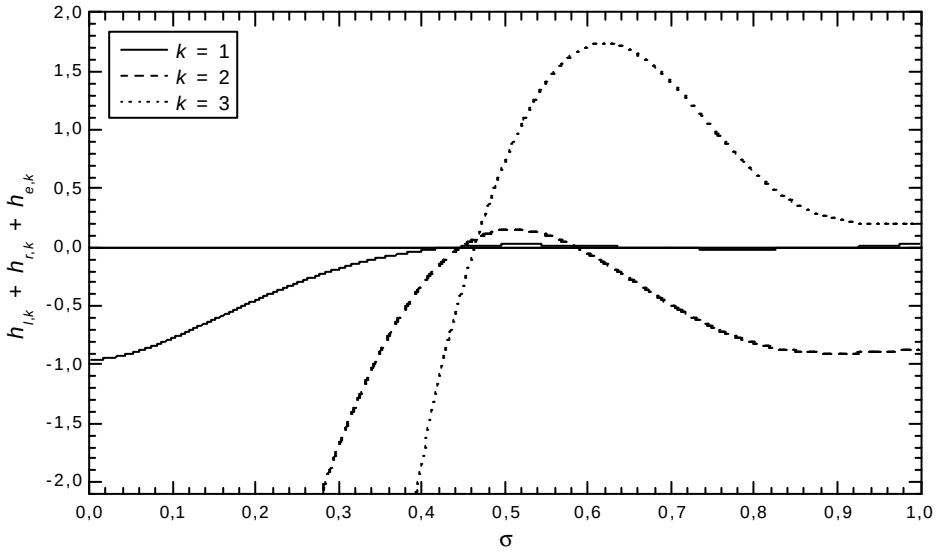

Fig. 6: Variation of the constant $\sum_j h_{j,k}$ with the sensors' distance for the lowest three modes considering the effect of all three added masses.

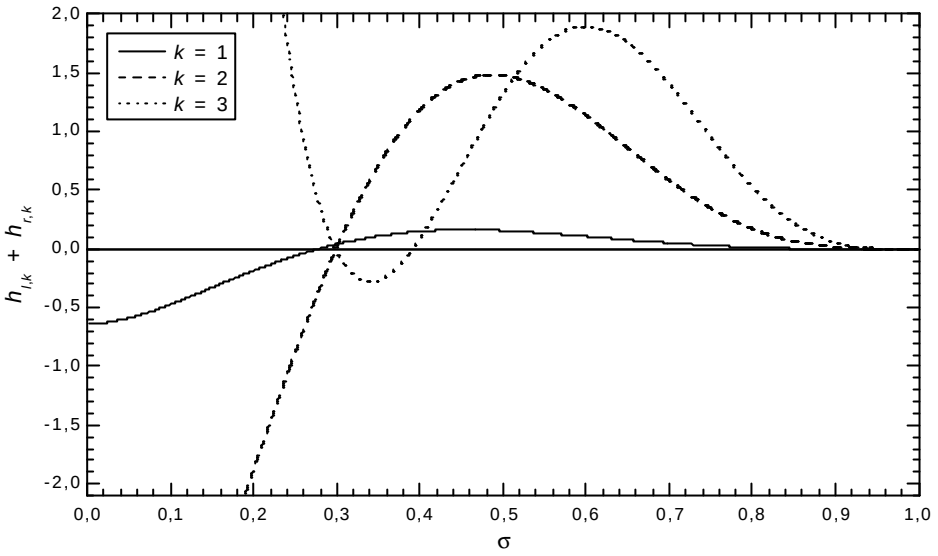

Fig. 7: Variation of the constant $\sum_j h_{j,k}$ with the sensors' distance for the lowest three modes considering the effect of two symmetrically located masses.

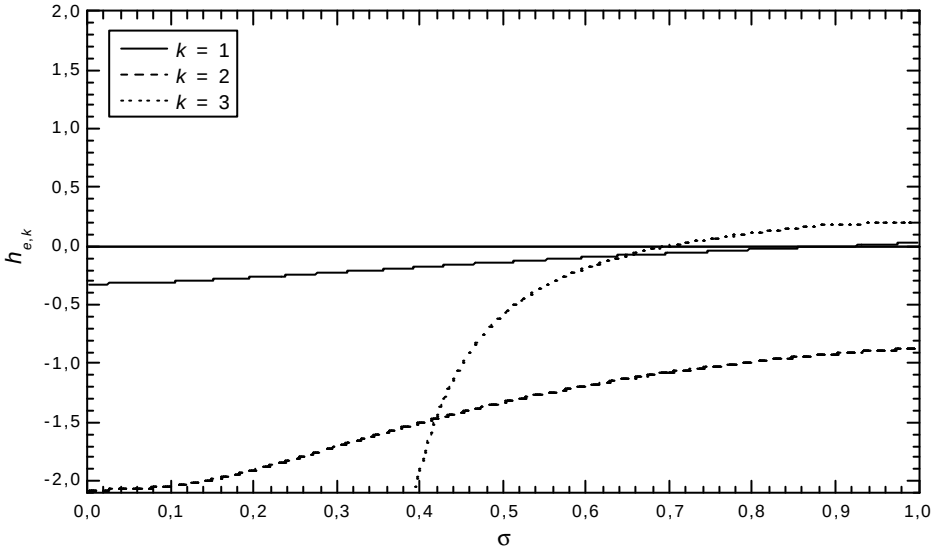

Fig. 8: Variation of the constant $\sum_j h_{j,k}$ with the sensors' distance for the lowest three modes considering the effect of one mass at the middle of the tube.

magnitude) larger non-idealities with respect to the fundamental mode. Also for k = 1, the added-masses effect is negligible in the wider range of σ, i.e. σ > 0.4, only for equal masses of the exciter and sensors (Fig. 6). Furthermore, the case of all three masses offers the only interesting region in the vicinity of $\sigma_{opt,k}$ for the second mode, too. But it has to be taken into account that this configuration is not realistic, since it is not likely that the exciter would be placed at the node of the mode shape, which is at the middle of the tube. In the third mode there is a zero influence of the added masses, found relatively close to the expected measuring distance, at σ = 0.70 for the single mass at the middle of the tube, i.e. for relatively small masses of the sensors. With the intention of determining the fluid-density effect, the relative change of the time difference in terms of two different fluid densities can be calculated:

$$\varepsilon_{\Delta\tau} = \frac{\Delta\tau_k\big|_{\beta_2} - \Delta\tau_k\big|_{\beta_1}}{\Delta\tau_k\big|_{\beta_1}} = \frac{\left(\dfrac{1}{1+\beta_2} - \dfrac{1}{1+\beta_1}\right)\sum_j h_{j,k}\alpha_j}{1 + \dfrac{1}{1+\beta_1}\sum_j h_{j,k}\alpha_j}, \tag{22}$$

which can be simplified for relatively small values of $\sum_j h_{j,k}\alpha_j$:

$$\varepsilon_{\Delta\tau} \approx \left(\frac{1}{1+\beta_2} - \frac{1}{1+\beta_1} \right) \sum_j h_{j,k}\alpha_j \,. \tag{23}$$

Let us consider a numerical example, e.g. $\sum_j h_{j,k}\alpha_j$ = 0.01, β_1 = 0.5 and β_2 = 1.5, which results in $\varepsilon_{\Delta\tau}$ = –0.26 %. Being aware that such a case is possible in practical configurations (e.g., α_j = 0.01, which means the added mass of 1 % of the tube mass and $\sum_j h_{j,k}$ = 1), so large non-idealities are certainly not insignificant for the new-generation Coriolis meters.

4. CONCLUSION

In this paper we describe a comparison of the straight-tube Coriolis meter's characteristics for the lowest three lateral vibration modes of the measuring tube. The study was based on the approximate, analytically expressed solutions of a one-dimensional mathematical model. In this way, the ideal characteristics and the effects of the stability boundary, the axial force and the added masses were discussed, and the following conclusions can be made:

- Under ideal conditions, the relative sensitivity of the natural frequencies on the fluid density remains unchanged for different vibration modes. However, the higher modes can contribute to the higher sensitivity of the mass-flowrate characteristic, if the phase difference is the measured parameter. At the same time, it has to be considered that the meter's sensitivity to the mass flowrate depends strongly on the sensors' position.
- The higher modes are also better in terms of the stability-boundary and the axial-force effects. Smaller non-idealities are the consequence of the higher critical velocities in the case of the higher modes.
- However, from the viewpoint of the added-masses effect, the mass-flowrate measurements in the higher modes become much more dependant on the fluid density than for the fundamental mode. If the magnitudes of the added masses of the exciter and sensors are not negligible, only the appropriate combinations and positions of the masses can reduce this effect to a certain degree.

APPENDIX

Constants of the homogeneous system of linear equations (Eq. (6)):

$$c_{mn} = \int_0^1 \varphi_m \varphi_n \mathrm{d}\xi,\ d_{mn} = \int_0^1 \varphi_m \frac{\mathrm{d}\varphi_n}{\mathrm{d}\xi}\mathrm{d}\xi,\ e_{mn} = -\int_0^1 \varphi_m \frac{\mathrm{d}^2\varphi_n}{\mathrm{d}\xi^2}\mathrm{d}\xi,\ f_{mn}(\xi_j) = \varphi_m(\xi_j)\varphi_n(\xi_j)\,, \tag{A.1}$$

with the analytically evaluated integrals:

$$\begin{aligned}
&m = n:\ c_{mm} = 1,\ d_{mm} = 0,\ e_{mm} = \lambda_m\sigma_m\left(\lambda_m\sigma_m - 2\right),\\
&m \neq n\ \ (m+n \text{ is even}):\ c_{mn} = d_{mn} = 0,\ e_{mn} = \frac{8\lambda_m{}^2\lambda_n{}^2}{\lambda_n{}^4 - \lambda_m{}^4}\left(\lambda_m\sigma_m - \lambda_n\sigma_n\right),\\
&m \neq n\ \ (m+n \text{ is odd}):\ c_{mn} = e_{mn} = 0,\ d_{mn} = \frac{-8\lambda_m{}^2\lambda_n{}^2}{\lambda_n{}^4 - \lambda_m{}^4}\,.
\end{aligned} \tag{A.2}$$

Constants of the ideal meter's characteristics (Eq. (9)):

$$g_{\Omega,k} = \lambda_k{}^2,\ h_{\Delta\tau,k} = \sum_m h^*_{\Delta\tau,km},\ h^*_{\Delta\tau,km} = \frac{4d_{mk}}{\lambda_m{}^4 - \lambda_k{}^4}\frac{\varphi_m(\xi_l)}{\varphi_k(\xi_l)}\,. \tag{A.3}$$

Constants of the meter's characteristics including the stability-boundary effect (Eq. (16)):

$$g_{cen,k} = \frac{e_{kk}}{\lambda_k{}^4},\ g_{cor,k} = 4\sum_n \frac{d_{nk}{}^2}{\lambda_n{}^4 - \lambda_k{}^4},\ h_{cen,k} = \frac{1}{h_{\Delta\tau,k}}\sum_m h^*_{\Delta\tau,km}h^*_{cen,km},\ h_{cor,k} = \frac{4\lambda_k{}^4}{h_{\Delta\tau,k}}\sum_m h^*_{\Delta\tau,km}h^*_{cor,km}\,,$$

$$h^*_{cen,km} = \sum_n \frac{e_{mn}}{\lambda_n^4 - \lambda_k^4}\frac{d_{nk}}{d_{mk}} + \sum_p \frac{e_{pk}}{\lambda_p^4 - \lambda_k^4}\left(\frac{d_{mp}}{d_{mk}} - \frac{\varphi_p(\xi_l)}{\varphi_k(\xi_l)}\right) - \frac{e_{kk}}{\lambda_m^4 - \lambda_k^4},$$

$$h^*_{cor,km} = \sum_n \frac{d_{nk}}{\lambda_n^4 - \lambda_k^4}\sum_p \frac{d_{np}}{\lambda_p^4 - \lambda_k^4}\left(\frac{d_{mp}}{d_{mk}} - \frac{\varphi_p(\xi_l)}{\varphi_k(\xi_l)}\right) - \frac{1}{\lambda_m^4 - \lambda_k^4}\sum_n \frac{d_{nk}^2}{\lambda_n^4 - \lambda_k^4} - \frac{1}{3}\left(\sum_n \frac{d_{nk}}{\lambda_n^4 - \lambda_k^4}\frac{\varphi_n(\xi_l)}{\varphi_k(\xi_l)}\right)^2. \quad \text{(A.4)}$$

Constants of the meter's characteristics including the added-masses effect (Eq. (21)):

$$h_{j,k} = \frac{\lambda_k^4}{h_{\Delta\tau,k}}\sum_m h^*_{\Delta\tau,km}h^*_{j,km}, \quad h^*_{jkm} = \sum_n \frac{f_{mn}(\xi_j)}{\lambda_n^4 - \lambda_k^4}\frac{d_{nk}}{d_{mk}} + \sum_p \frac{f_{pk}(\xi_j)}{\lambda_p^4 - \lambda_k^4}\left(\frac{d_{mp}}{d_{mk}} - \frac{\varphi_p(\xi_l)}{\varphi_k(\xi_l)}\right) - \frac{f_{kk}(\xi_j)}{\lambda_m^4 - \lambda_k^4}. \quad \text{(A.5)}$$

REFERENCES

[1] Bose, T., Derby, H. V., Levien, A. K., Pankratz, A. W.: Method and apparatus for measuring pressure in a Coriolis mass flowmeter. US Patent 5734112.

[2] Kutin, J., Bajsic, I.: Stability-boundary effect in Coriolis meters. Flow Measurement and Instrumentation 12 (2001) 65-73.

[3] Kutin, J., Bajsic, I.: An analytical estimation of the Coriolis meter's characteristics based on modal superposition. Flow Measurement and Instrumentation 12 (2002) 345-351.

[4] Raszillier, H., Durst, F.: Coriolis-effect in mass flow metering. Archive of Applied Mechanics 61 (1991) 192-214.

[5] Raszillier, H., Alleborn, N., Durst, F.: Mode mixing in Coriolis flowmeters. Archive of Applied Mechanics 63 (1993) 219-227.

[6] Lange, U., Levien, A., Pankratz, T., Raszillier, H.: Effect of detector masses on calibration of Coriolis flowmeters. Flow Measurement and Instrumentation 5 (1994) 255-262.

[7] Raszillier, H., Alleborn, N., Durst, F.: Effect of a concentrated mass on Coriolis flowmetering. Archive of Applied Mechanics 64 (1994) 373-382.

[8] Sultan, G.: Theoretical and experimental studies of the Coriolis mass flowmeter. Ph.D. Thesis, Cranfield Institute of Technology, 1990.